

**In-plane charge fluctuations in bismuth-sulfide superconductors**Anushika Athauda,<sup>1</sup> Junjie Yang,<sup>1</sup> Seunghun Lee,<sup>1</sup> Yoshikazu Mizuguchi,<sup>2</sup> Keita Deguchi,<sup>3</sup> Yoshihiko Takano,<sup>3</sup> Osuke Miura,<sup>2</sup> and Despina Louca<sup>1,\*</sup><sup>1</sup>*Department of Physics, University of Virginia, Charlottesville, Virginia 22904, USA*<sup>2</sup>*Tokyo Metropolitan University, Tokyo, 192-0397, Japan*<sup>3</sup>*National Institute for Materials Science, Tsukuba 305-0047, Japan*

(Received 17 February 2015; revised manuscript received 27 March 2015; published 22 April 2015)

The local atomic structure of the new nonmagnetic superconducting system  $\text{LaO}_{1-x}\text{F}_x\text{BiS}_2$  is investigated using neutron diffraction and the pair density function analysis. Evidence for local charge fluctuations linked to a charge disproportionation of the Bi ions in the distorted lattice of superconducting  $\text{LaO}_{1-x}\text{F}_x\text{BiS}_2$  is presented. In-plane short-range distortions of sulfur atoms up to 0.3 Å in magnitude break site symmetry and create two distinct environments around Bi. Out-of-plane motion of apical sulfur brings it closer to the La-O/F doping layer with increasing  $x$  that may lead to a charge transfer conduit between the doping layers and the superconducting  $\text{BiS}_2$  planes. The mechanism for superconductivity may arise from the interplay between charge density fluctuations and an enhanced spin-orbit coupling suggested theoretically that induces spin polarization.

DOI: [10.1103/PhysRevB.91.144112](https://doi.org/10.1103/PhysRevB.91.144112)

PACS number(s): 61.05.F-, 75.25.-j, 75.30.Ds, 78.70.Nx

The bismuth sulfide ( $\text{BiS}_2$ ) based superconductors [1–7] have attracted considerable attention recently because of the rich physics involving charge density wave (CDW) instability [8,9], atomic modes leading to phonon softening [8], and spin-orbit (SO) interactions with a hidden spin polarization [10]. Much of the recent interest in superconductors has been on materials whose parent ground state is magnetic, i.e., the Fe and Cu based systems. The  $\text{BiS}_2$  superconductors are not magnetic, possibly of the conventional type but with strong electronic correlations [11]. Density functional theory calculations suggested that spin polarization is present even though the crystal lattice is centrosymmetric [9,10], arising from the coupling of the electron orbital to its spin. SO coupling has been at the heart of spintronic physics and central to the mechanism of superconductivity that appears at the interfaces of  $\text{LaAlO}_3/\text{SrTiO}_3$  films [12], where a large Rashba SO coupling is important in stabilizing the superconducting state [13]. Given its quasi-two-dimensional crystal nature,  $\text{BiS}_2$  may exhibit SO coupling through the Dresselhaus effect as suggested by Ref. [10], which is the three-dimensional analog of the Rashba effect. This can happen without breaking crystal inversion symmetry but rather be driven by atomic site asymmetry [10].

In the two families of  $\text{BiS}_2$  superconductors,  $\text{Bi}_4\text{O}_4(\text{SO}_4)_{1-x}$  [1] and  $\text{LnO}_{1-x}\text{F}_x\text{BiS}_2$  ( $\text{Ln} = \text{La, Nd, Pr, Ce, and Yb}$ ) [2,14,15] discovered thus far, vacancies and crystal defects are common. Their structure is analogous to the  $\text{LaOFeAs}$  Fe-based superconductors, and superconductivity occurs in the  $\text{BiS}_2$  layers. While the  $\text{SO}_4$  layer carries vacancies in the former compound, the  $\text{LnO}_{1-x}\text{F}_x\text{BiS}_2$  system, the focus of this study, shows a peculiar relation of its crystal structure to superconductivity. The parent compound shows high crystallinity, and upon doping superconductivity appears at about 10% of F doping.  $T_C$  is maximized when crystal disorder is induced by high pressure annealing. The maximum  $T_C \sim 10$  K is reached at the  $x = 0.5$  doping

level under high pressure at which point the crystallinity is compromised [1,2]. When synthesized at ambient conditions, the  $x = 0.5$  reaches a  $T_C$  of 7 K [7]. The structural disorder is manifested in the Bragg peak broadening; however, what leads to the broadening is not understood at present. To this end, the relation of disorder and superconductivity is central towards understanding the enhancement of the transition temperature in the  $\text{BiS}_2$  superconductors. In this paper we focus on the atomic nature of the disorder. Disorder has been intensely studied in cuprates [16] and, earlier, in amorphous solids [17,18]. Typically, disorder shortens the coherence length, enhances thermal fluctuations, and induces vortex pinning but without long-range ordering into a vortex lattice [16,19]. Such a state has been argued to correspond to a vortex glass [20].

In this system, the dominant carriers are from the Bi  $6p$  orbitals that strongly hybridize with the S  $3p$  near the Fermi surface. A CDW instability arises from a  $(\pi, \pi, 0)$  mode which corresponds to in-plane displacements of S atoms (0.18 Å) around the M point [9]. At the same time, SO coupling has a considerable effect on the electronic band structure around the X point of the Brillouin zone. Without SO coupling, four bands cross below  $E_F$  in the optimally doped composition  $x \sim 0.5$ . With SO coupling, only two bands cross below  $E_F$ . SO coupling originates from the inversion asymmetry and creates an effective magnetic field that lifts the spin degeneracy [21]. Are the new Bi-based superconductors conventional BCS type or a new class of non-BCS type, yielding a new route to unconventional superconductivity? Here, we provide evidence for the latter by analyzing neutron scattering data. Our results provide the experimental evidence for in-plane short-range S distortions ( $\sim 0.3$  Å in magnitude) that lead to charge fluctuations around Bi. Crystal strain develops along the compressed  $c$  axis, but the out-of-plane S atoms move closer to the doping layers. The local distortions present in this system may be an experimental realization of a vortex pinning mechanism in the glassy state of a superconductor.

The samples were prepared as described in Refs. [1–3]. The samples exhibit a low  $T_C$  when synthesized at ambient conditions while  $T_C$  increases under high pressure

\*Author to whom correspondence should be addressed: [louca@virginia.edu](mailto:louca@virginia.edu)

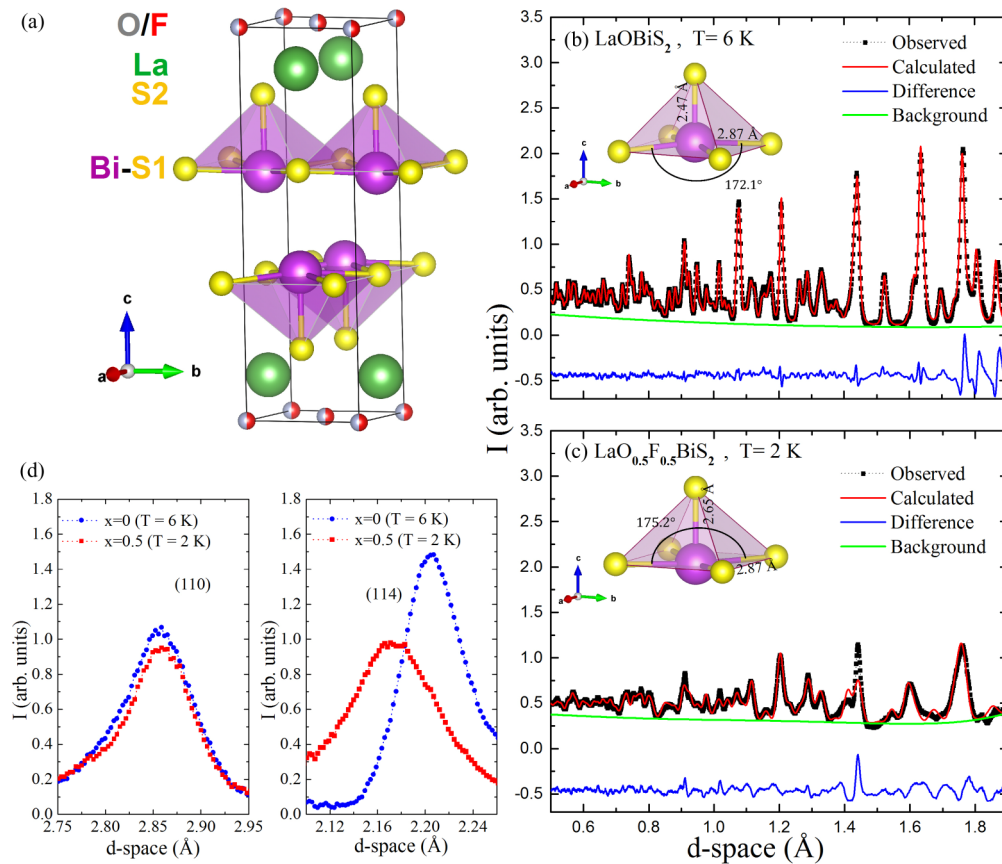


FIG. 1. (Color online) (a) The crystal structure of  $\text{LaO}_{1-x}\text{F}_x\text{BiS}_2$  with the BiS tetrahedra. (b) The neutron powder diffraction pattern (black symbols) of  $\text{LaOBiS}_2$  at 6 K was collected using NOMAD at the Spallation Neutron Source of Oak Ridge National Laboratory. The red, green, and blue solid lines represent the calculated intensity, background, and difference between the observed and calculated intensities, respectively. (c) The neutron powder diffraction pattern of  $\text{LaO}_{0.5}\text{F}_{0.5}\text{BiS}_2$  at 2 K has its intensity considerably reduced in comparison to the parent compound of (b). At the same time, the background (green solid line) has increased. (d) The comparison of the (110) and (114) Bragg peaks between the  $x = 0$  and  $x = 0.5$  compositions shows significant changes of the nonzero  $l$  peaks with  $x$ .

annealing [22]. The neutron diffraction experiment was carried out as a function of temperature and composition at the Nanoscale Ordered Materials Diffractometer (NOMAD) at the Spallation Neutron Source of Oak Ridge National Laboratory. The diffraction data were analyzed to obtain the total structure factor  $S(Q)$  that includes both Bragg and diffuse scattering. The  $S(Q)$  with a momentum transfer,  $Q = 37 \text{ \AA}^{-1}$ , was Fourier transformed to obtain the pair distribution function (PDF) that provides a real-space representation of atom-to-atom pair correlations. This analysis does not assume lattice periodicity. The same diffraction data were analyzed in reciprocal space using the Rietveld method, and the average structure can be described well using the tetragonal symmetry ( $P4/nmm$ ).

The quasi-two-dimensional layered crystal structure of  $\text{LaOBiS}_2$  shown in Fig. 1(a) consists of the superconducting  $\text{BiS}_2$  bilayers sandwiched between insulating  $\text{La}_2\text{O}_2$  blocking layers. The Bi ions form a square pyramidal edge shared lattice, coordinated by four in-plane (S1) and one out-of-plane (S2) sulfur ions. The plane is buckled with a S1-Bi-S1 bond angle of  $\sim 172.1^\circ$ . In the tetragonal symmetry, the base of the pyramid is a perfect square, and the Bi-S1 bonds are of the same length,  $2.87 \text{ \AA}$ . The out-of-plane Bi-S2 bond length of  $2.47 \text{ \AA}$  is significantly shorter. The substitution of oxygen ( $\text{O}^{2-}$ )

with fluorine ( $\text{F}^-$ ) in the blocking layers introduces electron carriers, and while the crystal symmetry  $P4/nmm$  does not change, the  $c$  axis contracts by 4% and the  $a$  axis expands by less than 0.2%. The  $\text{BiS}_2$  layer buckling is reversed with doping, in which the Bi ion moves away from the S2 atom, and the Bi-S2 bond length increases to  $2.65 \text{ \AA}$  by  $x = 0.5$ . The S1-Bi-S1 bond angle becomes  $184.8^\circ$  with a Bi-S1 bond of  $2.87 \text{ \AA}$ . This contradicts theoretical predictions that expect the lattice to become flat with doping [23].

The centrosymmetric space group does not change with doping [2], even though significant Bragg peak broadening along with diffuse scattering are observed in the neutron diffraction pattern [see Figs. 1(b) and 1(c) which compare the  $x = 0$  and  $x = 0.5$  samples]. It is perplexing how such a distorted crystal lattice is conducive to superconductivity. Earlier studies showed that the broadening affects Bragg peaks with nonzero  $l$  indices while Bragg peaks with  $l = 0$  are much sharper as reported in Ref. [24]. Figure 1(d) is a comparison of two nuclear Bragg peaks, the (110) and (114). The (114) Bragg peak and others with nonzero  $l$  become quite broad in the high pressure treated samples. This has been attributed to  $c$ -axis strain [22], arising from stacking faults in the presence of partial dislocations from imperfect stacking of crystal planes.

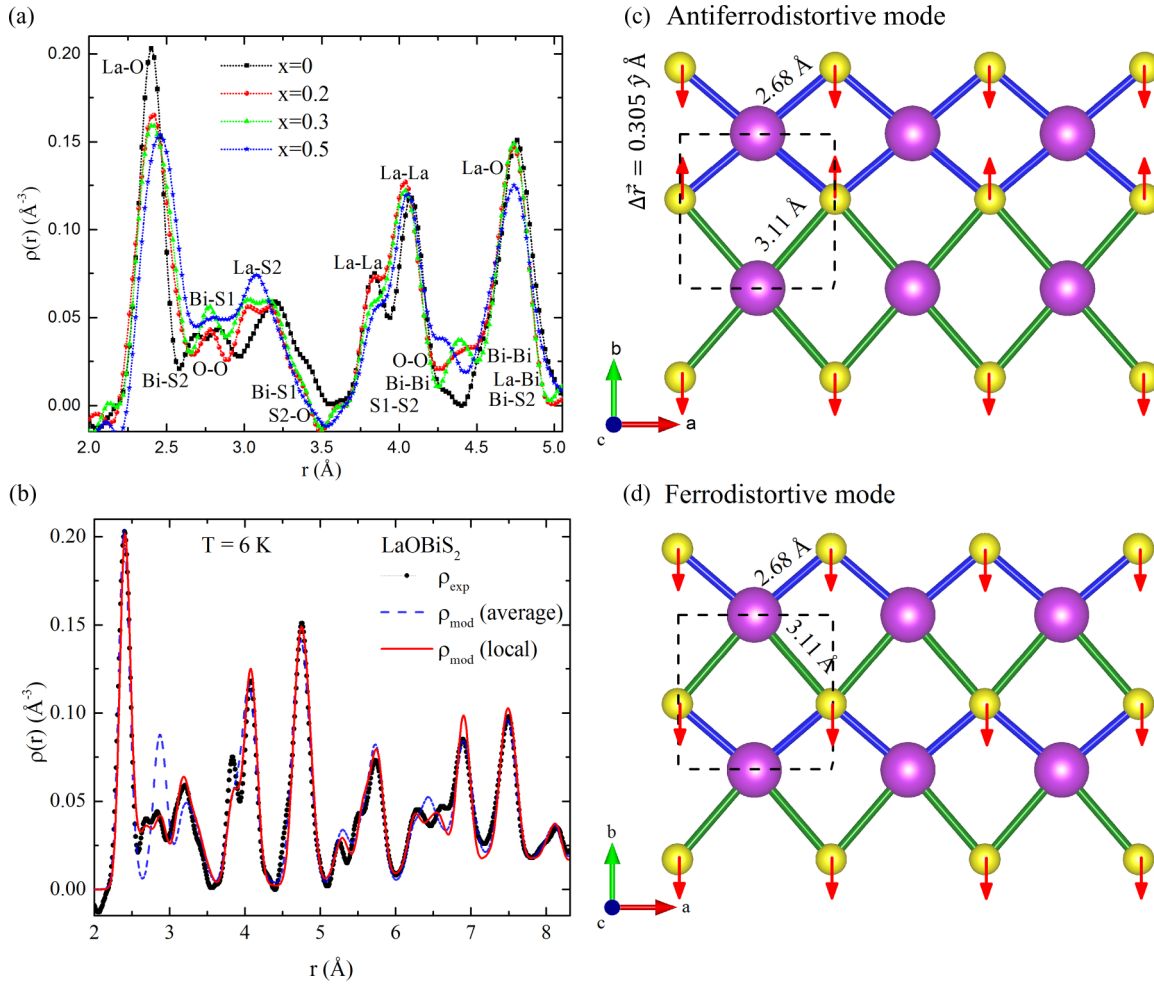


FIG. 2. (Color online) (a) A plot of the composition dependence of the data corresponding to the local structures of  $x = 0, 0.2, 0.3,$  and  $0.5$ . The data were collected at 6 K. (b) The PDF of the local structure for the parent compound at 6 K (black symbols) is compared to the average (dashed blue line) and local (solid red line) model PDFs. The agreement factor ( $A_{\text{factor}}$ ) between the local model and data is 0.156 while between the average model and data it is 0.283. (c) A schematic of the  $\text{BiS}_2$  plane showing the antiferrodistortive type mode. (d) A schematic of the  $\text{BiS}_2$  plane showing the ferrodistorptive type mode. The displacements of S1 are either in the  $x$  or  $y$  direction.

To investigate the origin of the broadening and diffuse scattering, here we use the real-space approach to extract the atom specific characteristics of the distortions and their real-space configuration. Bragg peak broadening and diffuse scattering can arise from other forms of defects besides stacking faults: The size mismatch between O and F can contribute to Huang scattering, for instance, while thermal diffuse scattering (TDS) due to phonons and static displacements of ions can additionally contribute to the diffuse scattering. We previously estimated the Debye temperature to be around 200 K for the  $x = 0.5$  [25] which indicates that TDS may not be insignificant in the temperatures of interest here,  $< 10$  K. The real-space atomic structure is represented in the PDF,  $\rho(r)$ . The  $\rho(r)$  is plotted in Fig. 2(a) for four compositions. This analysis provides the local arrangement of atoms and is very sensitive to short-range distortions. Further details can be found in Refs. [26] and [27]. The  $\rho(r)$  consists of correlation peaks that correspond to the probability of finding a particular pair of atoms, as labeled in the figure, at a given distance in space.

While in reciprocal space Bragg peak broadening is very pronounced as seen in Fig. 1(c), in real space, the PDF correlation peaks change shape with  $x$ , an unusual effect that indicates a local rearrangement is taking place that may be driven sterically and/or energetically. The crystal symmetry is invariant under doping and the differences observed in the PDFs of  $\text{LaO}_{1-x}\text{F}_x\text{BiS}_2$  cannot be explained by the substitution of  $\text{F}^-$  for  $\text{O}^{2-}$  as the two have very similar neutron scattering lengths and nominal ionic sizes. Starting with the parent compound, the PDF data is compared to a model  $\rho(r)_{\text{mod}}$ , calculated using the unit cell dimensions and atomic coordinates of the average structure. In Fig. 2(b),  $\rho(r)_{\text{exp}}$  (symbols) is compared to the model  $\rho(r)_{\text{mod}}$  (dashed blue line, average). The overall agreement between the two curves is good, however very clear differences are observed especially around 2.5–3.5  $\text{\AA}$  that are not due to systematic or statistical errors. Some ripples can be seen around the first PDF peak due to termination effects resulting from the truncation of the Fourier transform at a finite momentum transfer, but the aforementioned differences are well above the error.

In-plane S1 displacements can reproduce the local configuration that best fits the  $\rho(r)_{\text{exp}}$  of Fig. 2(b). The displacement modes are shown in Figs. 2(c) and 2(d). In Fig. 2(c), the displacement mode is of the antiferrodistortive type. Only S1 is displaced while all other atom coordinates are kept the same as in the average structure. A new  $\rho(r)_{\text{mod}}$  is calculated using the antiferrodistortive mode model and is compared to the  $\rho(r)_{\text{exp}}$  also in Fig. 2(b) (solid red line, local). In spite of its simplicity, this model fits the data quite well, especially in the 2.5 to 3.5 Å range. The antiferrodistortive mode shown in Fig. 2(c) creates short and long Bi-S1 bonds that affect the charge distribution around Bi. The distortion creates a double-well displacement potential of the Bi-S1 bonds. The data can be reproduced equally well using the displacement mode of Fig. 2(d). In this model, the S1 atoms are displaced in a ferrodistortive type mode, and create short and long Bi-S1 bonds in an asymmetric way. Both modes are equally likely as they give rise to identical magnitude of bonds. It is conceivable that both the ferrodistortive and antiferrodistortive type modes are locally present. The asymmetric coordination is reminiscent of the environment of Bi in  $\text{Cu}_4\text{Bi}_5\text{S}_{10}$  [28] due to the presence of a lone pair.

In the superconducting state, similar local modes are likely. The  $\rho(r)_{\text{exp}}$  of  $x = 0.5$  is shown in Fig. 3(a) and is compared

to the  $\rho(r)_{\text{mod}}$  for the average model of  $x = 0.5$  (dashed blue line) at 2 K. Differences are observed between the two in the same region of space as in the parent compound even though the shape of the PDF peaks are different. Just as in the parent compound, the antiferrodistortive and ferrodistortive modes can fit the data quite well [ $\rho(r)_{\text{mod}}$ 's shown in solid lines] but the magnitude of distortion is different. Shown in the inset of Fig. 3(a) are the Bi-S1 and Bi-S2 partial PDFs obtained from the local and average models for  $x = 0$  and  $x = 0.5$ . The bond lengths are also summarized in Table I. It can clearly be seen that the average Bi-S1 bond of 2.8 Å is split to two locally in both the  $x = 0$  and 0.5 while the split is larger in the  $x = 0$  than in  $x = 0.5$  sample. A third small peak is observed in close proximity to this bond that is from Bi-S1 bond lengths across planes.

The charge fluctuation inferred from the long and short Bi-S1 bond lengths is present in all compositions leading to the  $x = 0.50$  which is the only superconducting composition in our series. With doping, the Bi-S1 bonds differ in length as shown in the schematic of the Bi tetrahedra of Fig. 3(b). We can also see that upon entering the superconducting phase, the apical S2 atom gets further away from the planes and closer to the La(O/F) charge layers. The S2 atom can

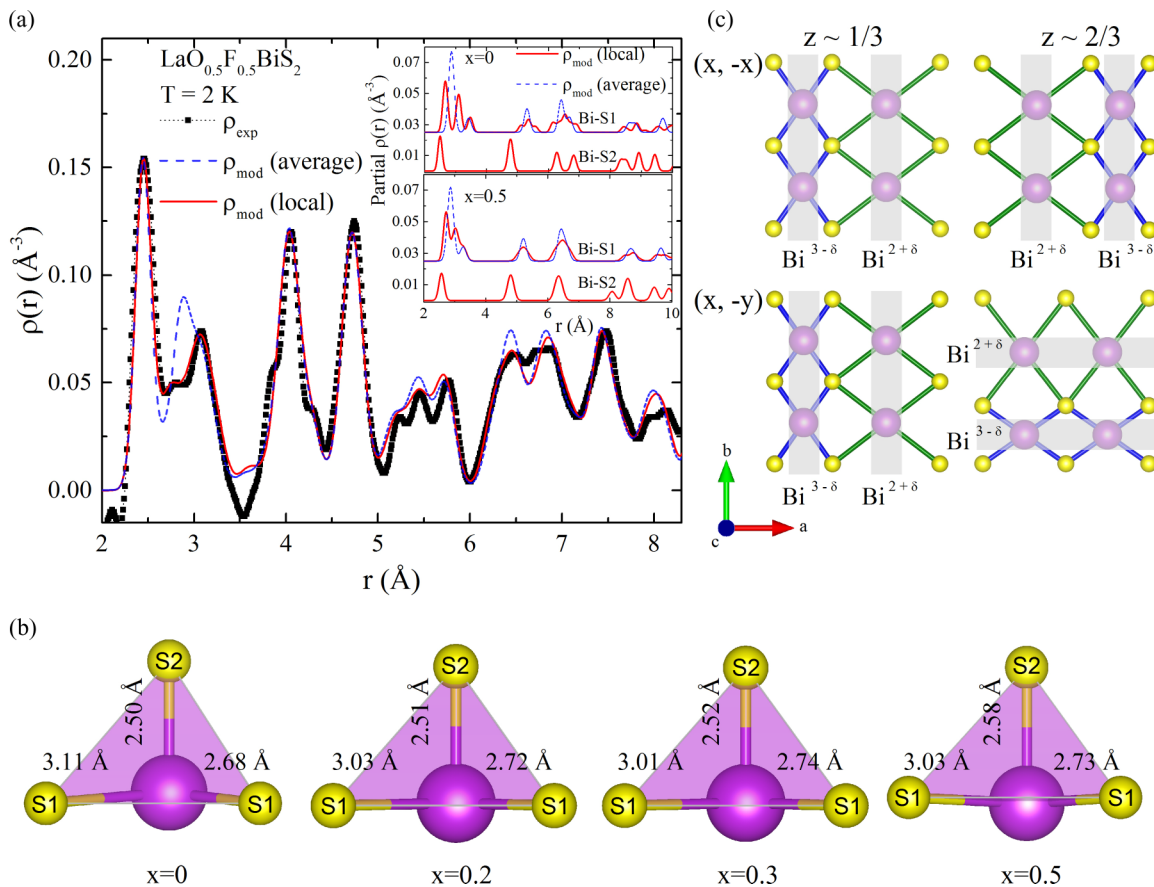


FIG. 3. (Color online) (a) The PDF of the local structure for  $x = 0.5$  at 2 K (black symbols) is compared to the average (dashed blue line) and local (solid red line) model PDFs. The  $A_{\text{factor}}$  between the local model and data is 0.18 while between the average model and data it is 0.239. The inset is a plot of the partial PDFs for Bi-S1 and Bi-S2 for  $x = 0$  (top) and  $x = 0.5$  (bottom). The partial of Bi-S1 for both the average and local models is shown while the partial of Bi-S2 is only shown for the local model. (b) A schematic of the Bi-S tetrahedron with the bond lengths determined from the refinement of the local structures of  $0 \leq x \leq 0.5$ . (c) Stripes of charge fluctuations in the two BiS<sub>2</sub> planes of the crystal structure. The  $(x, -x)$  and  $(x, -y)$  refer to the S1 coordinates in the  $z \sim 1/3$  and  $z \sim 2/3$  planes, respectively.

TABLE I. A list of the Bi-S bond lengths in the local structure.

	Bi-S1 bond length (Å)		Bi-S2 bond length (Å)
	Short	Long	
$x = 0, T = 6$ K	2.68	3.11	2.5
$x = 0.5, T = 2$ K	2.73	3.03	2.58

mediate the transfer of charge from the doping layers to the conduction  $\text{BiS}_2$  layers just like the chain oxygen does in  $\text{YBa}_2\text{Cu}_3\text{O}_{7-\delta}$  [29]. With temperature, the split of the Bi-S1 bonds in the  $x = 0.5$  changes little except upon approaching  $T_C$  where the split becomes larger [see Fig. 4(a)]. On the other hand, it is clear that with cooling, the height of the S2 atom gets closer to the donor planes [Fig. 4(b)]. This is also consistent with the temperature dependence of the height of S2 in the average structure although the values are different as seen in the figure.

The long and short Bi-S1 in-plane bonds indicate a variance in the Bi valence due to charge disproportionation. The proposed charge fluctuations are shown in the schematic of Fig. 3(c) for the  $\text{BiS}_2$  planes. Two displacement modes of the breathing type are tested: Given that there are two planes at  $z \sim 1/3$  and  $z \sim 2/3$ , in one mode the S1 distortions are in the  $(x, -x)$  direction in each plane, respectively, while in the other, the distortions are in the  $(x, -y)$  direction in each plane. Both modes yield the same local bond order but might be different energetically. Note that within one unit cell, the two  $\text{BiS}_2$  planes are rotated by 90 degrees. The  $(x, -x)$  only

breaks the fourfold rotational symmetry to a twofold while the inversion symmetry remains. The  $(x, -y)$  distortions break the fourfold and twofold rotational as well as the inversion symmetries.

The superconducting properties depend on structural defects and on their arrangement and knowing the average or ideal structure is not sufficient [30]. What can the local structure tell us about the crystal state of this new superconductor? It is clear that superconductivity is enhanced with the quenched disorder in this system and S1 and S2 distortions are important. Theoretical works have shown that a vortex-glass superconductor may be present in the bulk of disordered superconductors. In the presence of disorder, superconducting vortices can be pinned, preventing the formation of vortex lattices [16]. In analogy to the  $\text{BiS}_2$  superconductors, even though the  $\text{BiS}_2$  planes are distorted in the nonsuperconducting and superconducting samples, long-range structural order exists in the former as evidenced from the Bragg structure, and in the absence of pinning centers, the system can be in a vortex fluid phase with strong fluctuations preventing pairing. On the other hand, in the superconducting sample, the disorder is strong not only due to the distortions of the  $\text{BiS}_2$  planes but also due to the  $c$ -axis strain and stacking faults, allowing the system to enter the vortex glass thermodynamic state. The stripes of distortions proposed in Fig. 3(c) are *short-range* and the presence of stacking faults break the periodicity thus preventing any long-range order. It is possible that such modes can be the cause of vortex pinning.

The doping of  $\text{F}^-$  for  $\text{O}^{2-}$  changes the oxidation state of Bi nominally from 3+ to 2+ while introducing electron carriers. A simple estimate of the  $\text{Bi}^{3+}\text{-S}^{2-}$  bond length in the  $x = 0$  yields a value of  $\sim 2.8$  Å that is close to the bond length determined from the average structure. However, *locally*, the  $\text{Bi}^{3+}\text{-S}^{2-}$  bond lengths are split, as shown above. We cannot distinguish whether this is the result of an antiferrodistortive or a ferrodistortive type mode because they yield the same bond magnitude. The leading instability mode consists of displacements of S1 in the superconducting plane and out-of-plane S2 distortions. The in-plane distortions get smaller in the high pressure annealed  $x = 0.5$  superconducting samples while the out-of plane  $z$  motion of S2 increases. The two proposed modes will both create unequal charge distributions. However, such charge fluctuations are local and cannot produce a charge density wave. Even though this system is not magnetic, theoretical calculations showed that SO coupling leads to a hidden spin polarization that has a considerable effect on the electronic band structure around the X point of the Brillouin zone [10]. How the instability mode proposed here affects spin polarization will be interesting to investigate. In

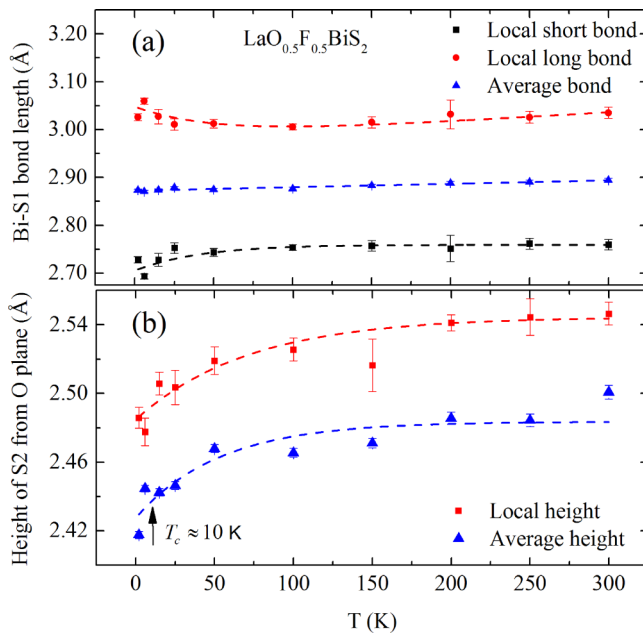


FIG. 4. (Color online) (a) The temperature dependence of the short (square) and long (circle) local Bi-S1 bond lengths is contrasted to the Bi-S1 average bond length (triangle). (b) The temperature dependence of the S2 atom from the oxygen plane obtained from fitting the data and from the Rietveld refinement of the average structure.

general, superconductivity in the presence of strong structural disorder might be a playing field for discovering exotic states [31,32].

The authors would like to thank X. Zhang, M. Hermely, and D. Dessau for useful discussions and B. Li for help with

the data reduction process. This work has been supported by the National Science Foundation, Grant No. DMR-1404994. Work at ORNL was supported by the U.S. Department of Energy, Office of Basic Energy Sciences, Materials Sciences and Engineering Division and Scientific User Facilities Division.

- 
- [1] Y. Mizuguchi, H. Fujihisa, Y. Gotoh, K. Suzuki, H. Usui, K. Kuroki, S. Demura, Y. Takano, H. Izawa, and O. Miura, *Phys. Rev. B* **86**, 220510(R) (2012).
- [2] Y. Mizuguchi, S. Demura, K. Deguchi, Y. Takano, H. Fujihisa, Y. Gotoh, H. Izawa, and O. Miura, *J. Phys. Soc. Jpn.* **81**, 114725 (2012).
- [3] S. Demura, Y. Mizuguchi, K. Deguchi, H. Okazaki, H. Hara, T. Watanabe, S. J. Denholme, M. Fujioka, T. Ozaki, H. Fujihisa, Y. Gotoh, O. Miura, T. Yamaguchi, H. Takeya, and Y. Takano, *J. Phys. Soc. Jpn.* **82**, 033708 (2013).
- [4] J. Xing, S. Li, X. Ding, H. Yang, and H.-H. Wen, *Phys. Rev. B* **86**, 214518 (2012).
- [5] H. Usui, K. Suzuki, and K. Kuroki, *Phys. Rev. B* **86**, 220501(R) (2012).
- [6] H. Kotegawa, Y. Tomita, H. Tou, H. Izawa, Y. Mizuguchi, O. Miura, S. Demura, K. Deguchi, and Y. Takano, *J. Phys. Soc. Jpn.* **81**, 103702 (2012).
- [7] K. Deguchi, Y. Mizuguchi, S. Demura, H. Hara, T. Watanabe, S. J. Denholme, M. Fujioka, H. Okazaki, T. Ozaki, H. Takeya, T. Yamaguchi, O. Miura, and Y. Takano, *Europhys. Lett.* **101**, 17004 (2013).
- [8] T. Yildirim, *Phys. Rev. B* **87**, 020506(R) (2013).
- [9] X. Wan, H.-C. Ding, S. Y. Savrasov, and C.-G. Duan, *Phys. Rev. B* **87**, 115124 (2013).
- [10] X. Zhang, Q. Liu, J.-W. Luo, A. J. Freeman, and A. Zunger, *Nat. Phys.* **10**, 387 (2014).
- [11] T. Zhou and Z. D. Wang, *J. Supercond. Nov. Magn.* **26**, 2735 (2013).
- [12] A. Ohtomo and H. Y. Hwang, *Nature (London)* **427**, 423 (2004).
- [13] A. D. Caviglia, M. Gabay, S. Gariglio, N. Reyren, C. Cantellieri, and J.-M. Triscone, *Phys. Rev. Lett.* **104**, 126803 (2010).
- [14] D. Yazici, K. Huang, B. D. White, A. H. Chang, A. J. Friedman, and M. B. Maple, *Philos. Mag.* **93**, 673 (2013).
- [15] B. Li, Z. W. Xing, and G. Q. Huang, *Europhys. Lett.* **101**, 47002 (2013).
- [16] D. S. Fisher, M. P. A. Fisher, and D. A. Huse, *Phys. Rev. B* **43**, 130 (1991).
- [17] W. L. Johnson, S. J. Poon, and P. Duwez, *Phys. Rev. B* **11**, 150 (1975), and references therein.
- [18] G. Kotliar and K. Kapitulnik, *Phys. Rev. B* **33**, 3146 (1986).
- [19] A. I. Larkin and Yu. N. Ovchinnikov, *J. Low Temp. Phys.* **34**, 409 (1979).
- [20] M. P. A. Fisher, *Phys. Rev. Lett.* **62**, 1415 (1989).
- [21] Q. Liu, Y. Guo, and A. J. Freeman, *Nano Lett.* **13**, 5264 (2013).
- [22] J. Kajitani, K. Deguchi, A. Omachi, T. Hiroi, Y. Takano, H. Takatsu, H. Kadowaki, O. Miura, and Y. Mizuguchi, *Solid State Commun.* **181**, 1 (2014).
- [23] A. Miura, M. Nagao, T. Takei, S. Watauchi, I. Tanaka, and N. Kumada, *J. Solid State Chem.* **212**, 213 (2014).
- [24] J. Lee, M. B. Stone, A. Huq, T. Yildirim, G. Ehlers, Y. Mizuguchi, O. Miura, Y. Takano, K. Deguchi, S. Demura, and S.-H. Lee, *Phys. Rev. B* **87**, 205134 (2013).
- [25] A. Athauda, J. Yang, B. Li, Y. Mizuguchi, S.-H. Lee, and D. Louca, *J. Supercond. Nov. Magn.* **28**, 1255 (2015).
- [26] T. Egami, Y. Petrov, and D. Louca, *J. Supercond.* **13**, 709 (2000).
- [27] D. Louca, E. L. Brosha, and T. Egami, *Phys. Rev. B* **61**, 1351 (2000).
- [28] L. A. Olsen, J. López-Solano, A. García, T. Balić-Žunić, and E. Makovicky, *J. Solid State Chem.* **183**, 2133 (2010).
- [29] M. Gupta and R. P. Gupta, *J. Phys. III France* **2**, 175 (1992).
- [30] J. D. Jorgensen, *Phys. Today* **44(6)**, 34 (1991).
- [31] B. Shalom, M. Sachs, D. Rakhmilevitch, A. Palevski, and Y. Dagan, *Phys. Rev. Lett.* **104**, 126802 (2010).
- [32] S.-T. Lo, S.-W. Lin, Y.-T. Wang, S.-D. Li, and C.-T. Liang, *Sci. Rep.* **4**, 5438 (2014).